Am J Transl Res 2025;17(2):1402-1415
www.ajtr.org /ISSN:1943-8141/AJTR0160785

Original Article

Mechanisms of *Picrasma quassioides* against hepatocellular carcinoma elucidated by network pharmacology and experimental validation

Jie Zhou[1], Zhilan Zhang[1], Ruiru Huang[1], Xingxing Zhuang[2], Shoudong Ni[1,2]

[1]*School of Pharmacy, Anhui Medical University, Hefei 230012, Anhui, China;* [2]*Department of Pharmacy, Chaohu Hospital of Anhui Medical University, Chaohu 238000, Anhui, China*

Received September 26, 2024; Accepted January 18, 2025; Epub February 15, 2025; Published February 28, 2025

Abstract: Objective: The medicinal plant *Picrasma quassioides* (*P. quassioides*) Benn exerts an inhibitory effect on the growth of hepatocellular carcinoma (HCC) cells via an unknown mechanism. This study explored the targets and signaling pathways underlying the mechanism of *P. quassioides* against HCC. Methods: Targets of *P. quassioides* active compounds were identified using the HERB database, and the HCC targets were found with the GeneCards database. The optimal serum concentration and intervention time were determined using the CCK-8 assay. Apoptosis, cell cycle, invasion, cloning, and wound-healing abilities were assessed using flow cytometry. Core protein targets and signaling pathway-related metabolic enzymes were evaluated with Western blotting. The anti-HCC effect of *P. quassioides* medicated serum was verified using arachidonic acid (AA)-related enzyme agonists. Results: Network pharmacology identified 19 effective compounds of *P. quassioides* and 105 HCC-associated targets. It also revealed the AA pathway was the central pathway of *P. quassioides* against HCC, with *AURKA*, *AURKB*, *KIF11*, and *TOP2A* identified as core targets that inhibit excessive HCC cell proliferation and promote apoptosis. Flow cytometry findings supported that *P. quassioides* medicated serum significantly inhibited HCC cell proliferation and promoted apoptosis. By contrast, enzyme agonists related to the AA pathway markedly counteracted the anti-HCC effect of *P. quassioides*, promoting HCC growth. Conclusion: *P. quassioides* medicated serum exerts a prominent anti-HCC effect in vitro. The AA pathway constitutes the mechanism by which *P. quassioides* medicated serum inhibits excessive proliferation and promotes apoptosis of HCC cells.

Keywords: *P. quassioides*, medicated serum, HCC, AA pathway, key targets

Introduction

Hepatoma, or hepatocellular carcinoma (HCC), is one of the leading causes of cancer-related deaths worldwide and is the only one among the top five most lethal forms of cancer that displays a yearly rise in prevalence [1]. Most of the world's estimated instances and fatalities stemming from HCC manifest in Eastern Asia (54.3% and 54.1%, respectively), which houses 21.5% of the planet's population. Specifically, China accounts for 45.3% of global HCC cases and 47.1% of HCC deaths [1, 2]. Effectively preventing and treating HCC represents a significant clinical obstacle, given the absence of efficacious medications and treatment modalities. Therefore, developing innovative therapeutic agents against this disease is of utmost concern to prevent increasing HCC deaths.

Picrasma quassioides (*P. quassioides*) Benn is a perennial herbaceous plant from the Simaroubaceae family [3], and its dried stems and branches are used for medicinal purposes. The main effective compounds extracted from *P. quassioides* are alkaloids and quassinoids, with the latter representing a group of highly oxygenated degraded terpenoids specific to the Simaroubaceae family. These compounds are biologically potent natural products with anti-inflammatory [4], antitumor [5], and neuroprotective activities [6]. For instance, β-carboline alkaloids [7] and tirucallane triterpenoids [8] extracted from *P. quassioides* promote HCC cell apoptosis and inhibit tumor growth; however, their mechanisms of action in treating HCC are vague. Because current progress in our understanding of *P. quassioides* antitumor effects comes from research on single compounds or

https://doi.org/10.62347/VLGD3371

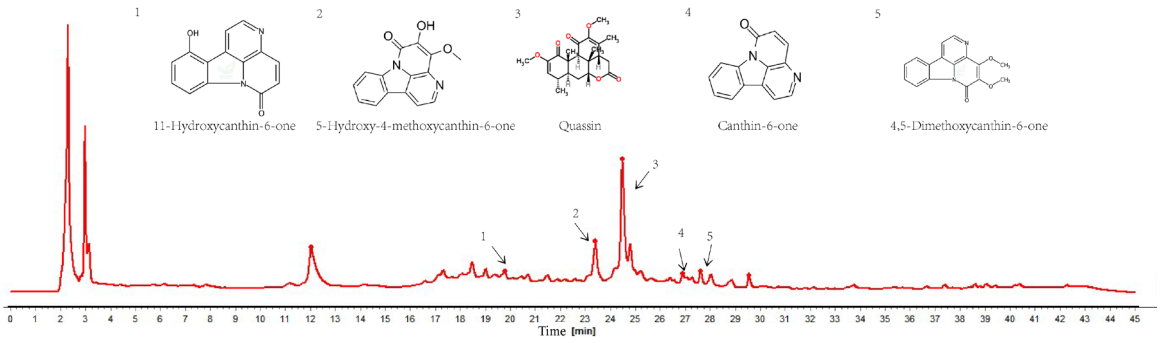

Figure 1. HPLC fingerprint of *P. quassioides*. HPLC: High Performance Liquid Chromatography.

their effects on treating diseases [9], a gap remains regarding the correlation between molecular targets, model pathways, and the anti-HCC activity of *P. quassioides* from a holistic perspective.

In this study, we used network pharmacology and in vitro experimental validation to investigate the possible pharmacological mechanism of *P. quassioides* in treating HCC. Specifically, we aimed to identify the key targets and signaling pathways involved in the anti-HCC effect of *P. quassioides* and offer novel insights for clinical development and application of this medicinal plant in HCC treatment.

Materials and methods

Preparation of P. quassioides medicated serum

Dried stems of *P. quassioides* (serial No. 051310101) were purchased from Anhui Weiwu Traditional Chinese Medicine Decoction Pieces Co., Ltd. (Bozhou, China). The stems were boiled in water at a 1:10 ratio (w/v) for 1 h, and the residue from the initial extraction was re-boiled at a 1:8 ratio (w/v) for 0.5 h. The solutions were mixed, filtered to eliminate solids, and concentrated to a final density of 0.63 g/mL before storing at 4°C for subsequent experiments. Quality control analysis was conducted using high-performance liquid chromatography (HPLC), and its fingerprint is depicted in **Figure 1**.

A total of 20 male 8-week-old Sprague-Dawley rats (270-300 g) were obtained from the Experimental Animal Center of Anhui *Medical University* and used for the animal experiments. The Medical Ethics Committee of Chaohu Hospital, affiliated with Anhui Medical University, approved the study and ensured it adheres to ethical standards for experimental animals (Approval No. KYXM-202403-012). The rats were placed in plastic cages with free access to standard feed and water and were left for 1 week to acclimatize before commencing the experiments. Following this period, the rats were assigned randomly to the *P. quassioides* group or the control group (n = 10 per group). Rats in the *P. quassioides* group were orally administered *P. quassioides* at 6.3 g/kg (equivalent to 6.3× the recommended clinical dose of 1 g/kg) once daily for 7 days, while those in the control group were given an equal quantity of saline solution. Upon the final administration, all rats were anesthetized with an intraperitoneal injection of urethane at 1.2 g/kg, and blood samples were drawn from the abdominal aorta. The serum obtained from the blood of each rat was centrifuged, merged, and filtrated through a 0.22-μm membrane and preserved at -80°C until further examination.

Cell culture, cell lines, and transfection

Human hepatocellular carcinoma cells HepG2 (CL-0103) were obtained from Procell Life Science & Technology Co., Ltd. (Wuhan, China) and maintained in a culture medium containing 10% fetal bovine serum and 1% penicillin-streptomycin at 37°C with 5% CO_2. After incubation, the cells were collected 24 h after treatment for further analysis.

Identification of P. quassioides active compounds

Bioactive ingredients targeting *P. quassioides* were identified with the HERB database (http://herb.ac.cn/) [10]. The screened ingredients

met Lipinski's principle: mass fraction ≤ 500, the logarithmic value of lipid-water partition coefficient < 5, number of hydrogen bond donors < 5, and number of hydrogen bond acceptors < 10. Subsequently, these ingredients were filtered using the SwissADME database (http://www.swissadme.ch/) to ensure retaining data with more than 3 positive results.

Identification of HCC-related genes

The GeneCards database (https://www.genecards.org/) provides comprehensive information on all annotated and predicted human genes. The database search applied the keyword "HCC" and identified 1787 HCC-associated target genes.

Establishment of a protein-protein interaction network

Potential gene targets for treating HCC with *P. quassioides* were recognized by finding overlapping candidates between 1787 HCC-associated genes and 19 *P. quassioides* active compounds using a Venn diagram. Topological information for protein-protein interaction network analysis was obtained from the STRING database (https://string-db.org/) by selecting interactions with a confidence score above 0.7. The network analysis included computing degree centrality.

Gene ontology and KEGG pathway enrichment analyses

Gene Ontology (GO) and Kyoto Encyclopedia of Genes and Genomes (KEGG) pathway enrichment analyses were conducted on the primary targets using the DAVID platform (https://david.ncifcrf.gov/). The platform allocated the official gene symbol as "OFFICIAL_GENE_SYMBOL", and *Homo sapiens* was selected as "organism". Statistical significance was determined with a $P < 0.05$ cutoff.

Molecular docking

The target protein structure was retrieved from the PDB database (https://www.rcsb.org), and the structure of the active compound was obtained from the PubChem database (https://pubchem.ncbi.nlm.nih.gov). Molecular docking was performed using AutoDock 4.0 software to determine the binding energy. Data visualization and mapping analysis were done with PyMOL 2.2.0 software.

Cell Counting Kit-8 (CCK-8) assay

Cells were seeded onto 96-well plates at a density of 1.0×10^5 cells per well, and the plates were transferred to an incubator for overnight incubation at 37°C in the presence of 5% CO_2. For culture medium replacement, 10% normal serum (Thermo Fisher Scientific, CA, USA) was combined with different concentrations of drug-containing serum or blank serum. The cultured cells were divided into 3 groups: control (culture medium), drug-containing serum (culture medium + drug-containing serum of varying concentrations), and blank serum (culture medium + blank serum). After culturing for various time lengths, each culture plate well was filled with 10 μL of CCK-8 solution and incubated for 60 min. The optical density at 450 nm was determined for each well.

Western blotting assay

Proteins were extracted from cell pellets with 100 μL Radio-Immunoprecipitation Assay (RIPA) solution containing 1 nM phenylmethylsulfonyl fluoride (PMSF). Subsequently, the extract was mixed with 5% sodium dodecyl sulfate-polyacrylamide gel electrophoresis (SDS-PAGE) at a 4:1 ratio and heated in boiling water for 10 min to denature proteins. The extract was allowed to cool for 30 min and subjected to SDS-PAGE. The separated proteins were transferred to a polyvinylidene difluoride membrane. The membranes were blocked with 5% skim milk for 2 h at room temperature and probed overnight at 4°C with primary antibodies. The primary antibodies were as follows: aurora kinase A (*AURKA*, 1:1000, DF8421); aurora kinase B (*AURKB*, 1:1000, AF0931); and DNA topoisomerase II alpha (*TOP2A*, 1:1000, AF02-39, Affinity Biosciences, Changzhou, China). Horseradish peroxidase-conjugated goat anti-rabbit IgG (1:10,000, ZB-2301) and goat anti-mouse IgG (1:10,000, ZB-2305) (Zs-BIO, Beijing, China) were added, and the membranes were incubated for 2 h at room temperature. Finally, the membranes were treated with a chemiluminescence detection kit (34094; Thermo Fisher Scientific, Shanghai, China), and band analysis was done with Image J software.

Scratch assay

Cells were spread onto a 6-well plate at approximately 1.0 × 10^6 cells per well, and 5 parallel scratches were made with a pipetting tip across the surface of cells. Plates were rinsed thrice with PBS (SH30256.01; Hyclone, Shanghai, China) to eliminate scratched cells and were supplemented with serum-free medium. Plates were placed to an incubator at 37°C with 5% CO_2 and cultured. Sampling and imaging were done at 0 and 24 h.

Cell cycle analysis

Cells were washed, trypsin digested, and centrifuged in pre-cooled PBS (SH30256.01; Hyclone, Shanghai, China) and fixed overnight at 4°C in 90% ethanol. The surfaces were cleaned with ethanol, and the fixed cells were returned to the PBS solution. Cells were treated with RNase at 37°C for 30 min, followed by incubation in darkness with the propidium iodide (PI) staining solution at 4°C for 30 min. Finally, flow cytometry was performed for cell cycle detection.

Apoptosis analysis

Cells adhered to culture plates were washed with ice-cold PBS (SH30256.01; Hyclone, Shanghai, China) and resuspended in AnnexinV-FITC/PI staining solution. They were incubated in the solution in darkness for 15 min, following the manufacturer's guidelines. The cells were filtered through a 200 mesh filter and examined by a flow cytometer (BD Biosciences, New Jersey, USA). An OLYMPUS inverted microscope (CKX53, Shanghai, China) was utilized to capture the image and NovoExpress was performed for apoptosis cell counting.

Invasion assay

Invasion assays were conducted using Transwell plates (724321; NEST, Wuxi, China). Diluted Matrigel (100 μL) was vertically added to the center of the bottom of the upper chamber. After incubation, the Transwell inserts were removed, and the non-invading cells on the upper membrane were wiped off carefully. Then, the inserts were fixed with 4% paraformaldehyde for 15 minutes at room temperature, washed twice with PBS before being stained with 0.1% crystal violet (C0121; Beyotime, Shanghai, China) for 20 minutes, and washed again with PBS until the background was clear. Images of three random areas were captured under an inverted microscope (CKX53, Olympus) and imported into NovoExpress for counting invading cells.

Clone formation assay

Cells at the logarithmic growth stage were treated with 0.25% trypsin and seeded onto 6-well plates at a concentration of 1 × 10^3 cells per well. Subsequently, they were incubated in a medium for 10 days. Cells were double rinsed with chilled PBS (SH30256.01; Hyclone, Shanghai, China) and fixed for 30 min in 4% paraformaldehyde. Developed cell colonies were dyed with 0.1% crystal violet for 1 h at 37°C and imaged by selecting 3 random visual fields under an inverted phase contrast microscope.

Statistical analysis

All experiments were repeated 3 times independently, and the study data were shown as mean ± standard deviation (mean ± SD). Statistical analysis was done using SPSS 22.0 software (IBM Corp., Armonk, NY, USA), and data visualization was conducted with GraphPad Prism software. Quantitative data underwent comparison using a 1-way ANOVA test. A $P < 0.05$ significance threshold was deemed statistically significant for all assessments. The figures displayed P values for each analysis, with $^{*}P < 0.05$ and $^{**}P < 0.01$ indicating statistical significance.

Results

Potential targets and pathways of P. quassioides against HCC

The HERB database was screened for active compounds of *P. quassioides* to describe its mechanism against HCC. A total of 19 active ingredients were identified (**Table 1**) and subjected to predictive search using the SwissTargetPrediction database. The search revealed 748 potential protein targets of the 19 active compounds, which were used to construct a composition-target network (**Figure 2A**). Next, the GeneCards database was examined using the keyword "HCC" and uncovered 1787 HCC-related target genes. These genes were overlapped with the 748 active ingredient targets of *P. quassioides* using Venn mapping,

Table 1. *P. quassioides* compound from HERB database

Compound	MW	XLOG	H donor	H acc
1-Acetyl-beta-carboline	210.23	2.3	1	2
Canthin-6-one	220.23	2.4	0	2
Quassin	388.5	2.4	0	6
S-(2-Carboxyethyl)-L-cysteine	193.22	-3.2	3	6
Nigakinone	226.25	2.1	1	3
1-Ethoxycarbonyl-beta-carboline	240.26	2.9	1	3
1-formyl-4-methoxy-beta-carboline	266.25	2.6	1	5
Astrapterocarpan	300.3	2.6	1	5
Nigakihemiacetal C	380.5	1.9	3	6
2,12-Dimethoxypicrasa-2,12-diene-1,11,16-trione	388.5	2.4	0	6
Isoquassin	388.5	2.4	0	6
Nigakihemiacetal A	410.5	1.2	3	7
Picrasin C	422.5	2.3	1	7
Nigakilactone C	434.5	3.1	0	7
Picropodophyllin-1-ethyl ether	442.5	2.9	0	8
Nigakilactone G	474.5	1.8	1	8
Methylnissolin	388.5	2.4	0	6
Picrasin G	390.5	2.2	1	6
(1S,2S,6S,8S,12R,14S,15S,19S,20S)-17-methoxy-7,15,19,20-tetramethyl-3,5,11-trioxapentacyclo[10.7.1.02,6.08,20.014,19]icos-16-ene-10,18-dione	390.5	2.9	0	6

Notes: MW: Molecular Weight; XLOG: Logarithmic value of fat-water partition coefficient; H donor: hydrogen donor; H acc: hydrogen acceptor.

revealing 105 key targets (**Figure 2B**). Finally, these targets were matched with the 19 active ingredients of *P. quassioides* for further analyses.

First, the 105 main targets were introduced into the STRING database to construct a protein-protein interaction network. The primary network (**Figure 2C**) included 105 nodes (i.e., proteins) and 355 edges (i.e., interactions). The leading 10 proteins, ordered according to the highest degree value, were *ESR1*, *PTGS2*, *JUN*, *CYP3A4*, kinesin family member 11 (*KIF11*), *AURKA*, *CYP1A2*, *CHBK1*, *TOP2A*, and *AURKB*.

The 105 primary targets were also subjected to GO and KEGG pathway enrichment analyses using the DAVID database to assess their functions and associated pathways. **Figure 3A** presents the top 10 targets and their corresponding enriched GO terms related to biological process (BP), molecular function (MF), and cell component (CC). In addition, **Figure 3B** summarizes the top 10 KEGG signaling pathways enriched with the primary targets. Finally, an active ingredient-target-pathway diagram (**Figure 3C**) was created to demonstrate the relationship between the 3 aspects.

Concentration and intervention time screening of P. quassioides medicated serum

The half-maximal inhibitory concentration (IC50) represents the drug concentration at which a biological process (e.g., cell proliferation) is inhibited by 50% and signifies a drug's efficacy. Hence, the IC50 values of *P. quassioides* medicated serum were determined along with the correlation among cell function, *P. quassioides* medicated serum levels, and treatment duration (**Figure 4A**). Findings from the CCK-8 assay showed that blank serum did not affect the proliferation ability of HepG2 cells. Conversely, medicated serums notably suppressed HepG2 cell proliferation compared to the blank serum ($P < 0.01$). Moreover, when cells were treated with 10% *P. quassioides* medicated serum for 72 h, the inhibition rate of cell proliferation approached 50% (IC50). As a result, 10% *P. quassioides* medicated serum and a 72-h intervention were selected for subsequent experiments.

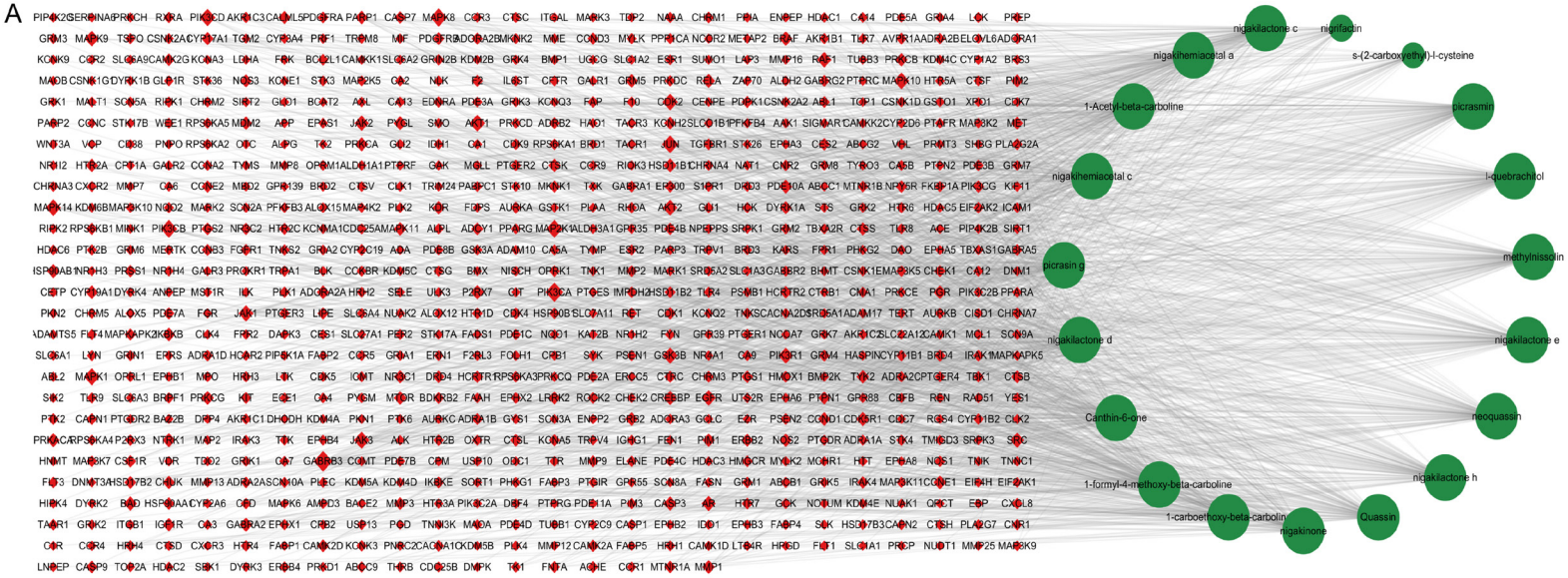
A
nigakillactone c
nigalactin
nigakihemiacetal a
s-(2-carboxyethyl)-l-cysteine
1-Acetyl-beta-carboline
picrasmin
nigakihemiacetal c
l-quebrachitol
picrasin g
methylnissolin
nigakillactone d
nigakillactone e
Canthin-6-one
neoquassin
1-formyl-4-methoxy-beta-carboline
nigakillactone h
1-carboethoxy-beta-carboline
Quassin
nigakinone

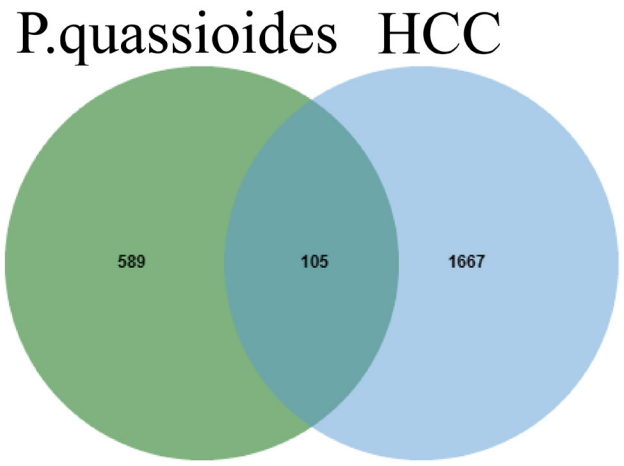
B
P.quassioides
HCC
589
105
1667

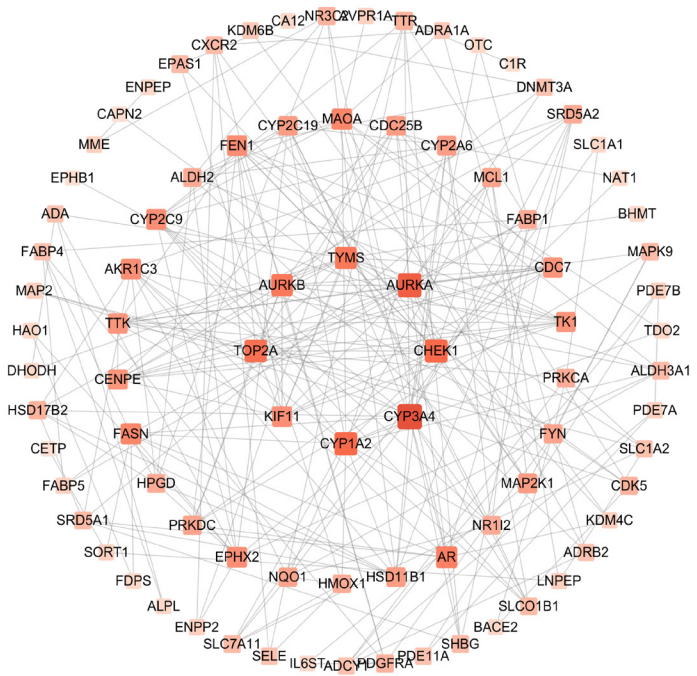
C
KDM6B
CA12
NR3C2
VPR1A
TTR
ADRA1A
CXCR2
OTC
EPAS1
C1R
ENPEP
DNMT3A
CAPN2
CYP2C19
MAOA
CDC25B
SRD5A2
MME
FEN1
CYP2A6
SLC1A1
EPHB1
ALDH2
MCL1
NAT1
ADA
CYP2C9
FABP1
BHMT
FABP4
TYMS
MAPK9
AKR1C3
CDC7
MAP2
AURKB
AURKA
PDE7B
HAO1
TTK
TK1
TDO2
TOP2A
CHEK1
DHODH
CENPE
PRKCA
ALDH3A1
HSD17B2
KIF11
CYP3A4
PDE7A
CETP
FASN
CYP1A2
FYN
SLC1A2
FABP5
HPGD
MAP2K1
CDK5
SRD5A1
PRKDC
NR1I2
KDM4C
SORT1
EPHX2
AR
ADRB2
FDPS
NQO1
HMOX1
HSD11B1
LNPEP
ALPL
SLCO1B1
ENPP2
BACE2
SLC7A11
SHBG
SELE
IL6ST
ADCY
PDGFRA
PDE11A

Figure 2. Network pharmacology analysis diagram. A. Component-target network diagram of *P. quassioides*. The green circles represent active ingredients, red diamond represents the targets. B. Venn map of *P. quassioides* targets and HCC targets. C. PPI of the common genes associated with *P. quassioides* and HCC. PPI: Protein-Protein Interaction; HCC: hepatocellular carcinoma.

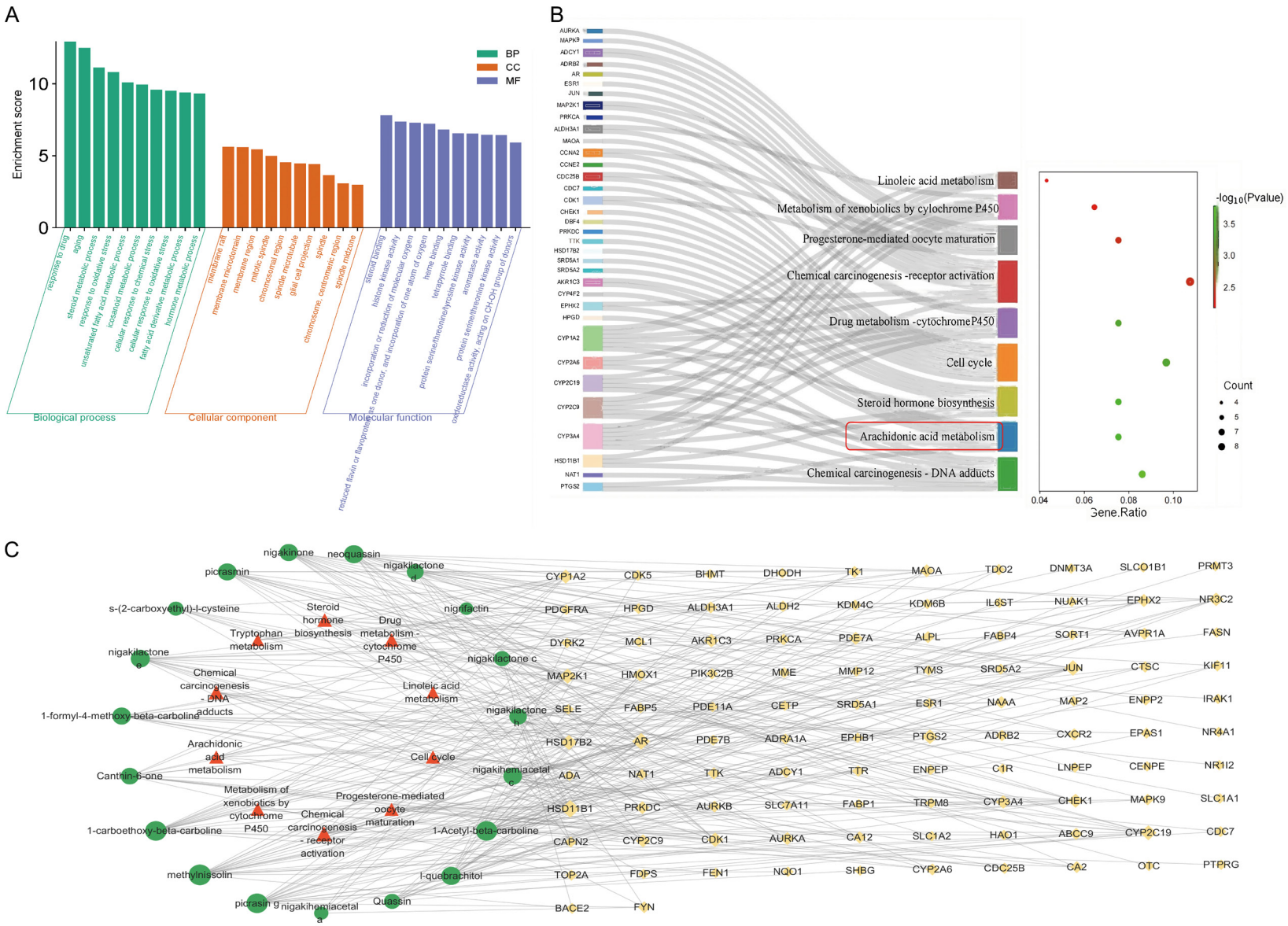

Figure 3. Network pharmacology analysis diagram. (A) GO and (B) KEGG analysis of the common genes associated with *P. quassioides* and HCC. (C) Active ingredients-Target-Pathway network. The green circles represent active ingredients, red triangle represents the pathway, yellow diamond represents the targets. GO: Gene Ontology; KEGG: Kyoto Encyclopedia of Genes and Genomes.

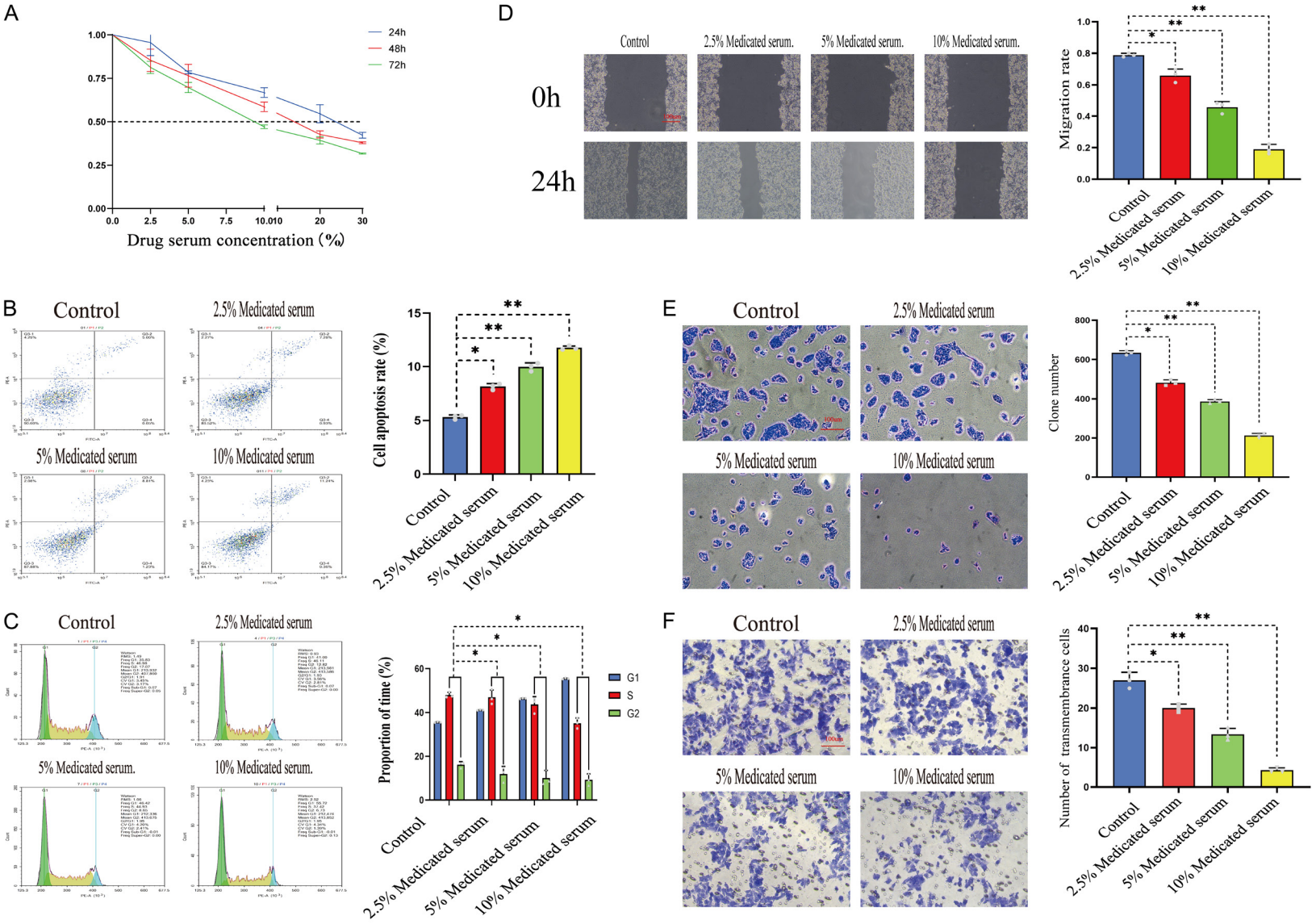

Figure 4. *P. quassioides* medicated serum inhibited excessive proliferation and promoted apoptosis of HCC. A. CCK-8 for the viability of HCC cells, 0-30% drug-containing serum concentration to detect cell viability at 24, 48 and 72 hours. B. Apoptosis plots of flow cytometry. The ratio of the second quadrant plus the fourth quadrant represents the ratio of cell apoptosis. C. Cell cycle diagram. The ratio of G2 phase plus S phase represents the proportion of cell proliferation. D. Cell scratch diagram. Cell migration rate of serum containing drugs at 0%, 2.5%, 5%, 10% concentrations at 0 and 24 hours. E. Cell cloning diagram. Number of cell clones cultured with 0%, 2.5%, 5%, 10% drug-containing serums after 10 days of culture. F. Transwell invasion assay diagram. The number of invading cells in the Transwell chamber at 0%, 2.5%, 5%, 10% concentrations. The graphs represent the average of 3 individual experiments, and the error bars denote the mean ± SD. $^{*}P < 0.05$, $^{**}P < 0.01$ compared to the control group. CCK-8: Cell Counting Kit-8; HCC: hepatocellular carcinoma.

Table 2. The binding energy of core genes and active ingredients

Core target	Active ingredients	Binding energy (kcal/mol)
AURKA	Nigakinone	-7.37
	Methylnissolin	-7.16
	Picrasmin	-7.60
	Picrasin G	-6.38
AURKB	Picrasin G	-9.38
	Nigakilactone e	-7.69
	1-Acetyl-beta-carboline	-7.09
	1-formyl-4-methoxy-beta-carboline	-6.78
KIF11	Methylnissolin	-6.76
	Quassin	-8.18
TOP2A	Canthin-6-one	-5.92

Notes: *AURKA*: aurora kinase A; *AURKB*: aurora kinase B; *KIF11*: kinesin family member 11; TOP2A: DNA topoisomerase II alpha.

P. quassioides medicated serum inhibits HepG2 proliferation and migration and promotes apoptosis.

How *P. quassioides* medicated serum affects the excessive proliferation and promoted apoptosis of HepG2 cells was investigated. Compared to control cells, an increase in early and late apoptotic HepG2 cells was detected in the *P. quassioides* group (**Figure 4B**). Moreover, the cell apoptosis rate progressively increased in the control group under 2.5%, 5%, or 10% *P. quassioides* medicated serum concentrations. These findings suggest that apoptosis is more pronounced when treating the cells with higher concentrations of *P. quassioides* medicated serum.

When the cell cycle was assessed in HepG2 cells (**Figure 4C**), the cell reproduction rate (S+G2) decreased under increasing concentrations of *P. quassioides*-containing serum. By contrast, the proportion of HepG2 cells in the reproductive phase decreased with rising drug-containing serum concentrations, aligning with the cell apoptosis results.

In addition, HepG2 cells were analyzed for their migratory ability (**Figure 4D**) with a scratch assay. After culturing HepG2 cells for 24 h, the scratches created in the cells from the *P. quassioides*-containing serum group were notably wider than those in the control group. Moreover, the cell migration rate decreased with elevated concentrations of drug-containing serum, indicating that the medicated serum hinders tumor cell migration.

Finally, HepG2 cells were exposed to different treatment conditions to investigate their colony-forming ability (**Figure 4E**). After 10 days of culture, the clonal inhibition rates of the cells in the 2.5%, 5%, or 10% medicated serum groups were significantly lower than the rates of the cells in the control group. A cell invasion assay (**Figure 4F**) uncovered that the number of cells penetrating the Transwell membrane decreased with increasing drug-containing serum concentrations compared with the control group.

Validation of network pharmacology results

Targets were ranked based on the scores of degree, betweenness, and closeness centralities using the cytoNCA plug-in in Cytoscape to identify the core targets (i.e., hub genes). The top 4 targets identified in the comprehensive ranking were as follows: *AURKA*, *AURKB*, *KIF11*, and *TOP2A*. Molecular docking was performed to verify the connections between these hub genes and the 19 essential active components of *P. quassioides*. The resulting connections between the key targets and the active components are displayed in **Table 2**. The binding energy between the key targets and their cor-

responding active elements was ≤ -5.0 kcal/mol, indicating strong binding activity. Each target and the compound that binds most effectively were illustrated with a detailed representation of the molecular docking mode shown in **Figure 5A**. The targets were verified with a Western blotting assay (**Figure 5B**), suggesting that their expression was inhibitory. Subsequent network pharmacology KEGG analysis suggested that *P. quassioides* might affect the arachidonic acid (AA) pathway. Therefore, whether the AA pathway has an impact on *P. quassioides* anti-HCC properties, the expression of 3 arachidonic acid-related metabolic enzymes was evaluated with Western blotting: cyclooxygenase 2 (COX2), arachidonate 5-lipoxygenase (LOX5), and cytochrome P450 family 4 subfamily A member (CYP4A) (**Figure 5C**). Indeed, the drug-containing serum of varying concentrations showed reduced expression of COX2 and LOX5 and enhanced CYP4A expression. Subsequently, a recovery experiment was conducted by adding a 0.1 mg/ml AA agonist to 10% of the drug-containing serum to validate that *P. quassioides* inhibits the AA pathway to suppress HCC formation. The additional scratch (**Figure 5D**), clone-forming (**Figure 5E**), and invasion (**Figure 5F**) assays demonstrated positive trends, supporting that *P. quassioides* inhibits HCC formation by targeting the AA pathway. In conclusion, the network pharmacology and in vitro findings suggest that the AA metabolic signaling pathway plays a crucial role in the ability of *P. quassioides* to inhibit HCC spread.

Discussion

This study utilized network pharmacology and in vitro cell experiments to verify the inhibitory effect of *P. quassioides* on HepG2 cells in hepatocellular carcinoma (HCC). It demonstrated that *P. quassioides* is effective in inhibiting HepG2 cell growth and identified the core targets and signaling pathways involved in the underlying mechanism. Specifically, the study identified *AURKA*, *AURKB*, *KIF11*, and *TOP2A* as core target genes of *P. quassioides*. Furthermore, it found that *P. quassioides* inhibits HCC growth by targeting crucial enzymes of the AA metabolic pathway. Evidence shows that some compounds extracted from *P. quassioides*, such as kumuquassin C and β-carboline-2-hydroxy-3-propionic acid, exhibit selective inhibitory activity on HepG2 cells and induce apoptosis in HCC [9, 10]. These results offer valuable insights into the clinical application of *P. quassioides* and present a promising avenue for treating HCC.

The *AURKA* and *AURKB* genes are known oncogenes that facilitate tumorigenesis in various solid and hematological malignant tumors. For example, the abnormal *AURKA* expression has been linked to its oncogenic function in tumorigenesis, which could be attributed to gene amplification, transcriptional activation, and hindered protein degradation in cancer tissues [11]. The *AURKB* gene, also known as *AIM-1* or *STK5*, participates in forming a chromosomal passenger complex along with inner centromere protein (INCENP), survivin, borealin/dasra, and other proteins [12]. This gene indirectly reduces the expression of the $p21^{WAF/CIP1}$ cell cycle inhibitor by restricting p53 activity to further cell cycle progression and hinder apoptosis [13]. Both *AURKA* and *AURKB* genes are associated with cancer cell expression, and inhibitory agents against their encoded proteins elicit cell demise [14]. Our analysis using network pharmacology of *P. quassioides* pinpointed *AURKA* and *AURKB* as target genes. Further experiments confirmed that the inhibitory effects of *P. quassioides* medicated serum were particularly potent in HepG2 cells on these targets. The *KIF11* gene is essential for the separation of duplicated poles and the maintenance of proper spindle bipolarity throughout mitosis [15]. It also plays a pivotal role in the transport of secretory proteins in nonmitotic cells [16] and in the regulation of axonal growth and branching in developing neurons [17]. This gene contributes to the proliferation and progression of different types of human cancers [18], and multi-omics studies underscore its significance in tumor initiation, progression, immune infiltration, and treatment response, suggesting *KIF11* potential as a pan-cancer biomarker [19]. Hence, the *KIF11* gene may be a valuable biomarker for predicting outcomes in immune, targeted, and chemotherapy treatments across different cancer types. The *TOP2A* gene is the third core target of *P. quassioides* identified in our study, and this gene controls cell division. It exhibits high expression levels during mitosis and has a vital role in mitotic chromosome condensation and segregation [20]. Evidence indicates that *TOP2A* con-

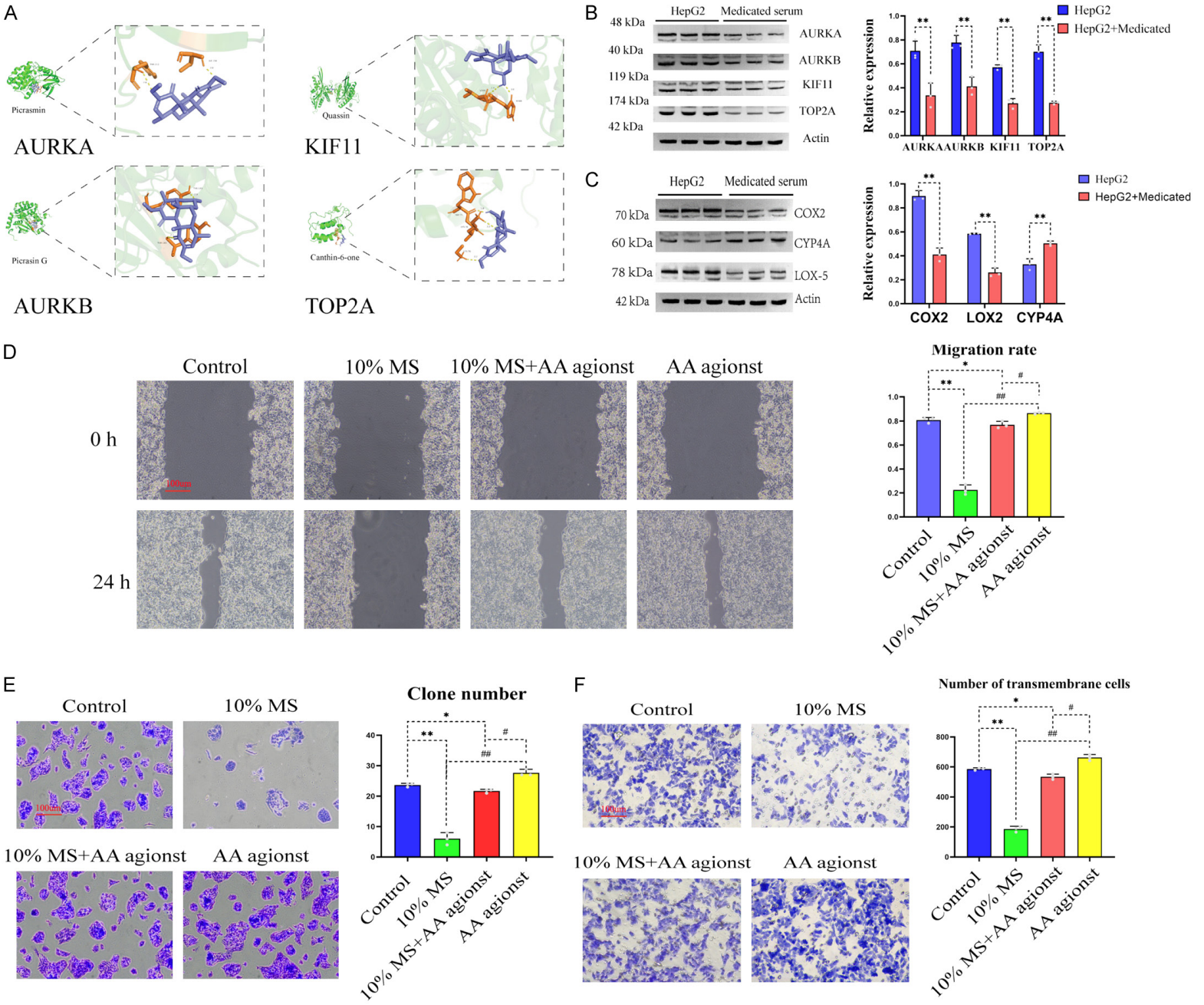
A
Picrasmin
AURKA
Quassin
KIF11
Picrasin G
AURKB
Canthin-6-one
TOP2A
B
HepG2
Medicated serum
48 kDa
40 kDa
119 kDa
174 kDa
42 kDa
AURKA
AURKB
KIF11
TOP2A
Actin
Relative expression
HepG2
HepG2+Medicated
AURKA
AURKB
KIF11
TOP2A
C
HepG2
Medicated serum
70 kDa
60 kDa
78 kDa
42 kDa
COX2
CYP4A
LOX-5
Actin
Relative expression
HepG2
HepG2+Medicated
COX2
LOX2
CYP4A
D
Control
10% MS
10% MS+AA agionst
AA agionst
0 h
24 h
Migration rate
Control
10% MS
10% MS+AA agionst
AA agionst
E
Control
10% MS
10% MS+AA agionst
AA agionst
Clone number
Control
10% MS
10% MS+AA agionst
AA agionst
F
Control
10% MS
10% MS+AA agionst
AA agionst
Number of transmembrane cells
Control
10% MS
10% MS+AA agionst
AA agionst

Figure 5. A. Molecular docking analysis of key targets with bioactive compounds (yellow is the docking part). B. Western blot and densitometric analysis of expression of *AURKA*, *AURKB*, *KIF11* and *TOP2A* cultured in medium containing 10% medicated serum or DMSO for 24 hours. C. Western blot and densitometric analysis of expression of *COX-2*, *CYP4A*, *LOX-5* cultured in medium containing 10% medicated serum or DMSO for 24 hours. D. Cell scratch diagram. Migration rate of cells in 0%, 10% medicated serum, 10% medicated serum + AA agonist, AA agonist for 24 hours. E. Cell cloning diagram. Cells were cultured for 10 days in 0%, 10% medicated blood, 10% medicated serum + AA agonist and AA agonist the number of cell clones. F. Transwell invasion assay diagram. The number of invading cells in the Transwell chamber at 0%, 10% concentrations, 10% medicated serum + AA agonist and AA agonist. The graphs represent the average of 3 individual experiments, and the error bars denote the mean ± SD. $^{*}P < 0.05$, $^{**}P < 0.01$ compared to the control group; $^{\#}P < 0.05$, $^{\#\#}P < 0.01$ compared to the model group. DMSO: dimethyl sulfoxide; AA: arachidonic acid.

tributes to the enhanced proliferation, migration, and invasion capabilities of HCC in vitro and in vivo. Additionally, the gene facilitates cells to transition from the G2 phase to the M phase of the cell cycle and promotes the epithelial-mesenchymal transition, advancing HCC progression [21]. Our study revealed that *P. quassioides* inhibits the proliferation and migration of HCC cells while promoting apoptosis. We hypothesize that this effect may be attributed to down-regulated *AURKA*, *AURKB*, *KIF11*, and *TOP2A* expression.

The AA metabolic pathway biosynthesizes various lipid mediators, participating in numerous physiological processes, such as inflammation and cancer. The essential enzymes of the pathway are phospholipase A2s (PLA2s), cyclooxygenases (COXs), lipoxygenases (LOXs), and cytochrome P450 monooxygenases (CYPs) [22]. The typical end products of the pathway are lysophospholipids, prostanoids, leukotrienes, hydroxyeicosatetraenoic acids, and epoxyeicosatetraenoic acids. Our Western blotting assays uncovered that COX2 and LOX5, 2 enzymes from the AA pathway, inhibit expression of the target molecule. Overexpression of COX2 promotes carcinogenesis, increasing the rate of cancer recurrence and reducing survival [23]. Additionally, the *COX2* transgene is a significant factor in the initiation of cancers such as HCC [24]. The LOX5 enzyme plays a crucial role in tumor adhesion and spread [25], with mounting evidence implying that inhibiting LOX5 activity suppresses tumor growth in various cancers [26, 27]. The inhibitory effect of *P. quassioides* medicated serum on these 2 proteins confirms that this medicinal plant suppresses HCC by inhibiting the AA pathway. By contrast, the serum had a promoting effect on the CYP4A enzyme in our Western blotting assays. The human *CYP4A* subfamily contains *CYP4A11* and *CYP4A22*, 2 closely related genes [28]. In a study [29] aimed at uncovering the connections between *CYP4A11* expression and the clinical implications of HCC, researchers investigated the levels of *CYP4A11* expression in 155 HCC cases. They observed that most non-neoplastic hepatocytes exhibited strong *CYP4A11* expression using immunohistochemistry, Western blotting, and RT-PCR. Despite the significant increase in *CYP4A* mRNA levels seen in thyroid, breast, colon, and ovarian cancers [30], the authors suggested that *CYP4A* expression may play a role in tumor progression in cancers characterized by abundant cancer desmoplasia. As a result, it facilitates invasion and interactions with tumor cells, which stands in contrast to the limited presence of cancer desmoplasia in most HCCs [29]. In conclusion, *P. quassioides* medicated serum inhibits 2 proteins of the AA pathway that promote HCC formation, suggesting the serum has a satisfactory inhibitory effect on HCC.

Conclusion

In this study, we investigated the anti-HCC effect of *P. quassioides* using network pharmacology and in vitro experimental verification. We found that the medicated serum of this plant potentially inhibits HCC by down-regulating the expression of *AURKA*, *AURKB*, *KIF11*, and *TOP2A* genes and inhibiting the AA metabolic pathway. A limitation of our study is that we only conducted network pharmacology analysis and cell experiments, without in vivo experimental validation. In addition, while we confirmed the impact of the AA pathway on HCC cells, further experiments are required to elucidate its mechanism. Despite these limitations, our study provides valuable insights into the inhibitory effects of *P. quassioides* on HCC cells, laying a foundation for future research.

Acknowledgements

We acknowledge the effort of all individuals involved in the work, which was supported by the Scientific Research Project of Anhui Commission of Health (AHWJ2021b043).

Disclosure of conflict of interest

None.

Address correspondence to: Shoudong Ni, Department of Pharmacy, Chaohu Hospital of Anhui Medical University, Chaohu 238000, Anhui, China. E-mail: nishoudong@ahmu.edu.cn

References

[1] Siegel RL, Miller KD and Jemal A. Cancer statistics, 2019. CA Cancer J Clin 2019; 69: 7-34.

[2] Rumgay H, Arnold M, Ferlay J, Lesi O, Cabasag CJ, Vignat J, Laversanne M, McGlynn KA and Soerjomataram I. Global burden of primary liver cancer in 2020 and predictions to 2040. J Hepatol 2022; 77: 1598-1606.

[3] Hamazaki Y, Kato M and Karasawa K. Methylnigakinone content determination and geographical origin discrimination for P. quassioides via fluorescence fingerprint and principal component analyses. J Pharm Biomed Anal 2022; 219: 114932.

[4] Shin NR, Shin IS, Jeon CM, Hong JM, Oh SR, Hahn KW and Ahn KS. Inhibitory effects of Picrasma quassioides (D.Don) Benn. on airway inflammation in a murine model of allergic asthma. Mol Med Rep 2014; 10: 1495-1500.

[5] Gong YX, Liu Y, Jin YH, Jin MH, Han YH, Li J, Shen GN, Xie DP, Ren CX, Yu LY, Lee DS, Kim JS, Jo YJ, Kwon J, Lee J, Park YH, Kwon T, Cui YD and Sun HN. Picrasma quassioides extract elevates the cervical cancer cell apoptosis through ROS-mitochondrial axis activated p38 MAPK signaling pathway. In Vivo 2020; 34: 1823-1833.

[6] He C, Wang Y, Yang T, Wang H, Liao H and Liang D. Quassinoids with insecticidal activity against Diaphorina citri Kuwayama and neuroprotective activities from Picrasma quassioides. J Agric Food Chem 2020; 68: 117-127.

[7] Zhao WY, Zhou WY, Chen JJ, Yao GD, Lin B, Wang XB, Huang XX and Song SJ. Enantiomeric β-carboline dimers from Picrasma quassioides and their anti-hepatoma potential. Phytochemistry 2019; 159: 39-45.

[8] Zhao WY, Chen JJ, Zou CX, Zhang YY, Yao GD, Wang XB, Huang XX, Lin B and Song SJ. New tirucallane triterpenoids from Picrasma quassioides with their potential antiproliferative activities on hepatoma cells. Bioorg Chem 2019; 84: 309-318.

[9] Zhao WY, Chen JJ, Zou CX, Zhou WY, Yao GD, Wang XB, Lin B, Huang XX and Song SJ. Effects of enantiomerically pure β-carboline alkaloids from picrasma quassioides on human hepatoma cells. Planta Med 2019; 85: 648-656.

[10] Fang S, Dong L, Liu L, Guo J, Zhao L, Zhang J, Bu D, Liu X, Huo P, Cao W, Dong Q, Wu J, Zeng X, Wu Y and Zhao Y. HERB: a high-throughput experiment-and reference-guided database of traditional Chinese medicine. Nucleic Acids Res 2021; 49: D1197-D1206.

[11] Du R, Huang C, Liu K, Li X and Dong Z. Targeting AURKA in cancer: molecular mechanisms and opportunities for cancer therapy. Mol Cancer 2021; 20: 15.

[12] Kim I, Choi S, Yoo S, Lee M and Park JW. AURKB, in concert with REST, acts as an oxygen-sensitive epigenetic regulator of the hypoxic induction of MDM2. BMB Rep 2022; 55: 287-292.

[13] González-Loyola A, Fernández-Miranda G, Trakala M, Partida D, Samejima K, Ogawa H, Cañamero M, de Martino A, Martínez-Ramírez Á, de Cárcer G, Pérez de Castro I, Earnshaw WC and Malumbres M. Aurora B overexpression causes aneuploidy and p21Cip1 repression during tumor development. Mol Cell Biol 2015; 35: 3566-78.

[14] Jiang J, Wang J, Yue M, Cai X, Wang T, Wu C, Su H, Wang Y, Han M, Zhang Y, Zhu X, Jiang P, Li P, Sun Y, Xiao W, Feng H, Qing G and Liu H. Direct phosphorylation and stabilization of MYC by aurora B kinase promote T-cell leukemogenesis. Cancer Cell 2020; 37: 200-215.e205.

[15] Gu X, Zhu Q, Tian G, Song W, Wang T, Wang A, Chen X and Qin S. KIF11 manipulates SREBP2-dependent mevalonate cross talk to promote tumor progression in pancreatic ductal adenocarcinoma. Cancer Med 2022; 11: 3282-3295.

[16] Luo Y, Liu W, Zhu Y, Tian Y, Wu K, Ji L, Ding L, Zhang W, Gao T, Liu X and Zhao J. KIF11 as a potential cancer prognostic marker promotes tumorigenesis in children with Wilms tumor. Pediatr Hematol Oncol 2022; 39: 145-157.

[17] Pandey H, Popov M, Goldstein-Levitin A and Gheber L. Mechanisms by which kinesin-5 motors perform their multiple intracellular functions. Int J Mol Sci 2021; 22: 6420.

[18] Hu ZD, Jiang Y, Sun HM, Wang JW, Zhai LL, Yin ZQ and Yan J. KIF11 promotes proliferation of hepatocellular carcinoma among patients with liver cancers. Biomed Res Int 2021; 2021: 2676745.

[19] Guo X, Zhou L, Wu Y and Li J. KIF11 as a potential pan-cancer immunological biomarker encompassing the disease staging, prognoses,

tumor microenvironment, and therapeutic responses. Oxid Med Cell Longev 2022; 2022: 2764940.
[20] Uusküla-Reimand L and Wilson MD. Untangling the roles of TOP2A and TOP2B in transcription and cancer. Sci Adv 2022; 8: eadd4920.
[21] Wang T, Lu J, Wang R, Cao W and Xu J. TOP2A promotes proliferation and metastasis of hepatocellular carcinoma regulated by miR-144-3p. J Cancer 2022; 13: 589-601.
[22] Dia B, Alkhansa S, Njeim R, Al Moussawi S, Farhat T, Haddad A, Riachi ME, Nawfal R, Azar WS and Eid AA. SGLT2 inhibitor-dapagliflozin attenuates diabetes-induced renal injury by regulating inflammation through a CYP4A/20-HETE signaling mechanism. Pharmaceutics 2023; 15: 965.
[23] Höing B, Kanaan O, Altenhoff P, Petri R, Thangavelu K, Schlüter A, Lang S, Bankfalvi A and Brandau S. Stromal versus tumoral inflammation differentially contribute to metastasis and poor survival in laryngeal squamous cell carcinoma. Oncotarget 2018; 9: 8415-8426.
[24] Chen H, Cai W, Chu ESH, Tang J, Wong CC, Wong SH, Sun W, Liang Q, Fang J, Sun Z and Yu J. Hepatic cyclooxygenase-2 overexpression induced spontaneous hepatocellular carcinoma formation in mice. Oncogene 2017; 36: 4415-4426.
[25] Cox TR, Gartland A and Erler JT. Lysyl oxidase, a targetable secreted molecule involved in cancer metastasis. Cancer Res 2016; 76: 188-192.
[26] Merchant N, Bhaskar LVKS, Momin S, Sujatha P, Reddy ABM and Nagaraju GP. 5-Lipoxygenase: its involvement in gastrointestinal malignancies. Crit Rev Oncol Hematol 2018; 127: 50-55.
[27] Vaezi MA, Safizadeh B, Eghtedari AR, Ghorbanhosseini SS, Rastegar M, Salimi V and Tavakoli-Yaraki M. 15-Lipoxygenase and its metabolites in the pathogenesis of breast cancer: a double-edged sword. Lipids Health Dis 2021; 20: 1-19.
[28] Saito T, Honda M, Takahashi M, Tsukada C, Ito M, Katono Y, Hosono H, Saigusa D, Suzuki N, Tomioka Y, Hirasawa N and Hiratsuka M. Functional characterization of 10 CYP4A11 allelic variants to evaluate the effect of genotype on arachidonic acid ω-hydroxylation. Drug Metab Pharmacokinet 2015; 30: 119-122.
[29] Eun HS, Cho SY, Lee BS, Kim S, Song IS, Chun K, Oh CH, Yeo MK, Kim SH and Kim KH. Cytochrome P450 4A11 expression in tumor cells: a favorable prognostic factor for hepatocellular carcinoma patients. J Gastroenterol Hepatol 2019; 34: 224-233.
[30] Alexanian A, Miller B, Roman RJ and Sorokin A. 20-HETE-producing enzymes are up-regulated in human cancers. Cancer Genomics Proteomics 2012; 9: 163-169.